Eur. Phys. J. B **13**, 305–312 (2000)

THE EUROPEAN PHYSICAL JOURNAL B

EDP Sciences

A neural network model composed of two-state and three-state neurons

Y. Nakamura[1,a] and A.R. Ferchmin[2]

[1] School of Informatics and Sciences, Nagoya University, Nagoya, 464-8601, Japan
[2] Institute of Molecular Physics, Polish Academy of Sciences, ul. Smoluchowskiego 17, 60-179 Poznań, Poland

Received 26 October 1998 and Received in final form 12 February 1999

Abstract. A neural network model composed of two-state (1 and -1) and three-state (1, 0 and -1) neurons is proposed. The two-state neurons are connected with the three-state ones only and *vice versa*. We derive dynamic equations for the model under the assumption of non-symmetrical dilution of connections. A zero-noise phase diagram is obtained and a region in which two fixed point solutions can coexist is found. Basins of attraction for the solutions are also investigated.

PACS. 05.45.-a Nonlinear dynamics and nonlinear dynamical systems – 87.80.Xa Neural engineering

1 Introduction

In recent years, there has been a great deal of research on neural networks and many kinds of models have been proposed. Originally, behaviors of neurons were mostly described by either binary or continuous variables [1,2]. Recently, however, neural networks composed of other types of neurons are attracting interest from the point of view of biology and applications. For example, oscillator neural networks are inspired by some experimental results [3]. Theoretical investigations of this kind of models have been performed by several authors [4–7]. Neural networks with multistate neurons such as Potts type neurons [8–10] or multiple-level Ising (Q-Ising) type ones [11–14] are also proposed. The merit of the latter type of models is that one neuron can be correlated with a complex state such as a color or a grey tone of each pixel in an image. Moreover, a neural network model composed of multidimensional spin neurons was proposed [15] as a general extension of the Hopfield model of theoretical interest.

Most of the networks proposed so far, though, were assumed to be homogeneous, which means that networks consisted of only one kind of elements. To our knowledge, only a few models composed of two kinds of elements or more have been discussed; a network consisting of neurons with a sigmoidal or a piecewise linear input-output relation [16], a network of oscillators with scattered natural frequencies [17], and an Ashkin-Teller neural network with two types of interacting neurons at each site having different functions [18]. In this paper, we consider yet another network composed of two kinds of neuron-like elements, which are two-state or three-state ones. One of the questions we want to answer is whether or not the network shows new interesting properties. Therefore we investigate static and dynamic properties of this model stressing the pure physics rather than any possible biological background.

The rest of this paper is organized as follows: in Section 2, we introduce our model composed of two kinds of neurons. We derive equations which govern the dynamics of the system in Section 3. On the basis of the results of Section 3, we calculate the phase diagram and discuss the static properties in Section 4. In Section 5, we solve numerically equations derived in Section 3 and investigate the dynamic properties of the present system. Basins of attraction are also discussed. In the last section (Sect. 6), we summarize our results.

2 Model

Although in this paper we concentrate upon a network composed of two-state ($S = \frac{1}{2}$) and three-state ($S = 1$) neurons, let us first define a more general model composed of two kinds of neurons both of which in general take three states $(+1, 0, -1)$, however, with different thresholds. Note that if the threshold is equal to zero, neurons take only two states $(+1, -1)$. Two types of neurons, say, type-A neurons and type-B neurons, are distributed in the nodes of a bipartite lattice in such a way that each type-A neuron contacts only with type-B neurons *via* synaptic connections J_{ij} and *vice versa*. If they were nearest neighbors, the network could look like that in Figure 1 in the paper by Kaneyoshi [19], but they are not. The connections are essentially global, but with a bipartite connectivity like that in the paper by De Wilde [20]. Non-symmetrical dilution of the connections is assumed [21], which leads ultimately to closed dynamic equations. Let us define $S_i^f (f = A \text{ or } B)$

[a] e-mail: yasuyuki@info.human.nagoya-u.ac.jp

as a state of i-th neuron belonging to a subnetwork f, where the subnetwork f consists of $N/2$ type-f neurons. The interactions (connections) J_{ij} between pairs of neurons i and j are expressed in terms of the p embedded patterns ξ_i^μ ($\mu = 1, \ldots, p; i = 1, \ldots, N$) as

$$J_{ij} = \frac{C_{ij}}{C} \sum_{\mu=1}^{p} \xi_i^\mu \xi_j^\mu, \tag{1}$$

where the random parameters C_{ij} (independent of C_{ji}) take the value 1 with probability $\frac{2C}{N}$ and 0 with probability $1 - \frac{2C}{N}$. The network will be treated in the extreme dilution limit [21] $(\ln N)/(\ln C) \to \infty$ for $N \to \infty$. J_{ij} are assumed to be non-zero only between pairs of neurons belonging to different subnetworks. Half of neurons of the pattern ξ_i^μ ($i = 1, \ldots, N$) are of type-A and the other half of type-B. Without loss of generality, we apply the notation admitting that the variables S_i^f and ξ_i^μ with $1 \le i \le N/2$ belong to the type-A and S_i^f and ξ_i^μ with $N/2+1 \le i \le N$ belong to the type-B. Each pattern has an activity a_μ^A on the A-subnetwork defined by

$$a_\mu^A = \frac{2}{N} \sum_{i=1}^{N/2} |\xi_i^\mu| \tag{2}$$

and, on the B-subnetwork,

$$a_\mu^B = \frac{2}{N} \sum_{i=1}^{N/2} |\xi_{N/2+i}^\mu|. \tag{3}$$

For active neurons in a pattern, we assume that $\xi_i^\mu = 1$ or -1 with equal probability.

The model proposed here is a generalization of that proposed by Yedidia [11] applying identical Q-Ising spin variables with $Q = 3$ on the whole network. We adopt discrete time parallel dynamics and as an updating rule, the state of the i-th neuron belonging to the subnetwork f at the next time step is defined as

$$S_i^f(t+1) = \begin{cases} 1 \text{ with probability } \exp[(h_i^f(t) - \theta_f)/T]/Z_f \\ 0 \text{ with probability } 1/Z_f \\ -1 \text{ with probability } \exp[(-h_i^f(t) - \theta_f)/T]/Z_f \end{cases} \tag{4}$$

with $Z_f \equiv \exp[(h_i^f(t) - \theta_f)/T] + 1 + \exp[(-h_i^f(t) - \theta_f)/T]$ for $\theta_f \neq 0$ and

$$S_i^f(t+1) = \begin{cases} 1 \text{ with probability } \exp[h_i^f(t)/T]/Z_f \\ -1 \text{ with probability } \exp[-h_i^f(t)/T]/Z_f \end{cases} \tag{5}$$

with $Z_f \equiv \exp[h_i^f(t)/T] + \exp[-h_i^f(t)/T]$ for $\theta_f = 0$, where $h_i^f(t)$ is the local field at time t defined as

$$h_i^f(t) = \sum_j J_{ij} S_j^{f'}(t), \tag{6}$$

θ_f is a threshold for type-f neurons and T is the temperature. Note that $f' = A$ if $f = B$ and *vice versa*.

In our model we introduce an overlap for each subnetwork as follows. m_f^μ (f is A or B) denotes the overlap of the subnetwork f with pattern μ at time t and is defined as

$$m_A^\mu(t) = \frac{2}{N a_\mu^A} \sum_{i=1}^{N/2} \xi_i^\mu S_i^A(t) \tag{7}$$

and

$$m_B^\mu(t) = \frac{2}{N a_\mu^B} \sum_{i=1}^{N/2} \xi_{N/2+i}^\mu S_{N/2+i}^B(t). \tag{8}$$

A dynamic activity $a_D^f(t)$ is defined for the subnetwork f with $\theta_f \neq 0$,

$$a_D^f(t) = \frac{2}{N} \sum_i |S_i^f(t)|. \tag{9}$$

For $\theta_A = \theta_B$ one recovers the original Yedidia model [11], for $\theta_A = \theta_B = 0$ – one of the conventional models with two-level neurons. In order to have a model leading to closed formulas, our generalization of Yedidia's [11] work has been treated in the limit of non-symmetrical dilution with the help of the random independent parameters C_{ij} by applying the methods introduced for two-state neurons by Derrida *et al.* [21]. Since the latter paper is rather concise, the calculations presented in the form given by Kree and Zippelius [22] were followed closely. It has been carefully checked that all mathematics is correct also in the present mixed neurons case. In particular, our dynamic equations (see Eqs. (11-13) below) reduce in the $\theta_A = \theta_B = 0$ limit (*i.e.*, all neurons of two-level type) to those given in the Appendix A, p. 209 in the latter publication [22].

3 Equations

In this section, we present the dynamic equations of a mixed system consisting of two types of neurons f ($f = A$ or B) with, in general, different thresholds θ_f. In the special case of, say, $\theta_A = 0$, the system is reduced to a bipartite network with binary and three-level neurons. In the following, we consider the case when the network has some macroscopic overlap with one of the patterns (say, pattern 1) and no macroscopic overlap with any other one:

$$m_f^1 = m_f, \quad m_{f'}^1 = m_{f'}, \quad m_f^\nu = m_{f'}^\nu = 0 \quad (\nu \ge 2). \tag{10}$$

A calculation along the lines described in reference [22] for parallel dynamics leads to the following dynamic equations:

$$m_f(t+1) = \int_{-\infty}^{\infty} \frac{\mathrm{d}y}{\sqrt{2\pi L_{f'}(t)}} \exp\left(-\frac{y^2}{2L_{f'}(t)}\right) f_-[m_{f'}(t) - y; \theta_f] \tag{11}$$

and

$$a_D^f(t+1) = a_1 \int_{-\infty}^{\infty} \frac{\mathrm{d}y}{\sqrt{2\pi L_{f'}(t)}} \exp\left(-\frac{y^2}{2L_{f'}(t)}\right) f_+\left[m_{f'}(t)-y;\theta_f\right] + (1-a_1)\int_{-\infty}^{\infty} \frac{\mathrm{d}y}{\sqrt{2\pi L_{f'}(t)}} \exp\left(-\frac{y^2}{2L_{f'}(t)}\right) f_+\left[-y;\theta_f\right], \quad (12)$$

where

$$f_\pm[X;\theta] = \frac{\exp[(X-\theta)/T] \pm \exp[(-X-\theta)/T]}{\exp[(X-\theta)/T] + 1 + \exp[(-X-\theta)/T]}, \quad (13)$$

$L_f(t) = \alpha a_p^2 a_D^f(t)$ with the storage ratio $\alpha = \frac{p}{C}$ and $a_p^2 = \frac{1}{p-1}\sum_{\mu\geq 2} a_\mu^2$ and $f = A$ if $f' = B$ and *vice versa*.

We will be particularly interested in the case when one of the parameters, say, $\theta_A = 0$, thus defining a system composed of a mixture of two-level and three-level formal neurons. Therefore, in the following, we rename the variables. Namely, we replace the labels A and B with $\frac{1}{2}$ and 1, respectively. The label $\frac{1}{2}$ comes from spin-$\frac{1}{2}$ (two-state) neurons and the label 1 from spin-1 (three-state) neurons. For example, $S_i^{\frac{1}{2}}$ represent two-state neurons and S_i^1 three-state neurons. $m_{\frac{1}{2}}^\mu$ is the overlap with the pattern μ for the subnetwork composed of two-state neurons and m_1^μ is the one for the subnetwork composed of three-state neurons. Of course, the activities and dynamic activities of the subnetwork of two-state neurons are equal to unity. Thus we consider activities and dynamic activities only for the subnetwork of three-state neurons and we omit labels 1 for those variables. Specifically, we define activities of the part of three-state neurons of pattern μ as

$$a_\mu = \frac{2}{N}\sum_i |\xi_i^\mu| \quad (14)$$

and dynamic activities as

$$a_D(t) = \frac{2}{N}\sum_i |S_i^1(t)|. \quad (15)$$

Note that a similar kind of two-component model could be formulated with the use of general Q-level variables [23,24] with $Q > 3$. Now, if we set the threshold values $\theta_A = 0$ and $\theta_B = \theta$, the dynamic equations (11-12) take the following simplified form:

$$m_{\frac{1}{2}}(t+1) = \int_{-\infty}^{\infty} \frac{\mathrm{d}y}{\sqrt{2\pi L_1(t)}} \exp\left(-\frac{y^2}{2L_1(t)}\right) \tanh\left[\frac{m_1(t)-y}{T}\right], \quad (16)$$

$$m_1(t+1) = \int_{-\infty}^{\infty} \frac{\mathrm{d}y}{\sqrt{2\pi L_{\frac{1}{2}}}} \exp\left(-\frac{y^2}{2L_{\frac{1}{2}}}\right) f_-\left[m_{\frac{1}{2}}(t)-y;\theta\right] \quad (17)$$

and

$$a_D(t+1) = a_1 \int_{-\infty}^{\infty} \frac{\mathrm{d}y}{\sqrt{2\pi L_{\frac{1}{2}}}} \exp\left(-\frac{y^2}{2L_{\frac{1}{2}}}\right) f_+\left[m_{\frac{1}{2}}(t)-y;\theta\right] + (1-a_1)\int_{-\infty}^{\infty} \frac{\mathrm{d}y}{\sqrt{2\pi L_{\frac{1}{2}}}} \exp\left(-\frac{y^2}{2L_{\frac{1}{2}}}\right) f_+\left[-y;\theta\right], \quad (18)$$

where $f_\pm[X;\theta]$ is given by equation (13), $L_{\frac{1}{2}} = \alpha a_p^2$ and $L_1(t) = \alpha a_p^2 a_D(t)$ with the storage ratio $\alpha = p/C$ and $a_p^2 = \frac{1}{p-1}\sum_{\mu\geq 2} a_\mu^2$. Let us recall that our model differs from that presented in reference [16] in several aspects. First, it represents a mixture of two sorts of time-dependent variables (formal neurons): binary (two-level) and three-level ones. Second, from the two possible extremes of a random mixture, like in reference [16], and a completely ordered mixture, we choose the latter. Finally, as contrasted to the fully connected network of reference [16], we have the asymmetrically diluted model, for which one can derive closed evolution equations. The magnetic analogue of our system (except for dilution and range of connections) is a ferrimagnet [19] with two interpenetrating lattices of $S = \frac{1}{2}$ and $S = 1$ spins.

4 Static properties

Let us consider static properties of the system in the case of $T = 0$. From the dynamic equations (16-18), fixed point equations at zero noise have been derived to be

$$m_{\frac{1}{2}} = \mathrm{erf}\left(\frac{m_1}{a\sqrt{2\alpha a_D}}\right), \quad (19)$$

$$m_1 = \frac{1}{2}\left[\mathrm{erf}\left(\frac{m_{\frac{1}{2}}-\theta}{a\sqrt{2\alpha}}\right) + \mathrm{erf}\left(\frac{m_{\frac{1}{2}}+\theta}{a\sqrt{2\alpha}}\right)\right] \quad (20)$$

and

$$a_D = \frac{a}{2}\left[2 + \mathrm{erf}\left(\frac{m_{\frac{1}{2}}-\theta}{a\sqrt{2\alpha}}\right) - \mathrm{erf}\left(\frac{m_{\frac{1}{2}}+\theta}{a\sqrt{2\alpha}}\right)\right] + (1-a)\left[1 - \mathrm{erf}\left(\frac{\theta}{a\sqrt{2\alpha}}\right)\right], \quad (21)$$

where

$$\mathrm{erf}\left(\frac{x}{\sqrt{2}}\right) \equiv \sqrt{\frac{2}{\pi}}\int_0^x \exp\left(-\frac{z^2}{2}\right)\mathrm{d}z. \quad (22)$$

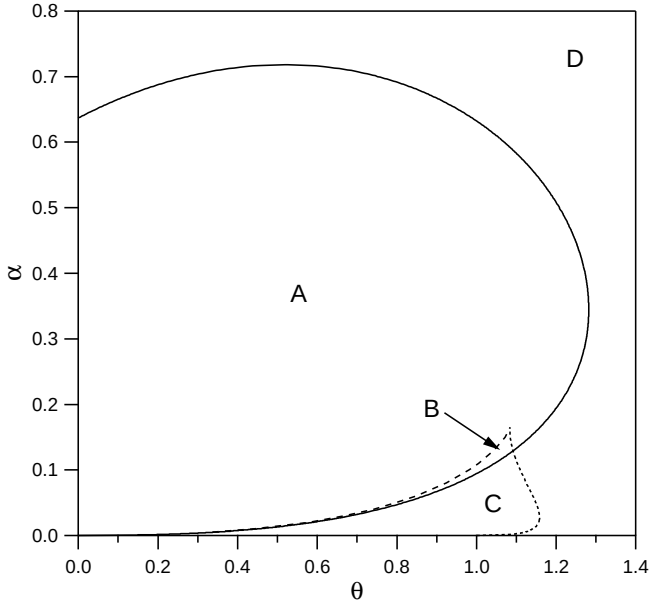

Fig. 1. The phase diagram in the parameters plane α *vs.* θ. The global storage ratio $M > 0$ in the regions A, B, and C; $M = 0$ in the region D. Solid line represents continuous (second order) transition, and dotted and dashed lines – the discontinuous (first order) transition.

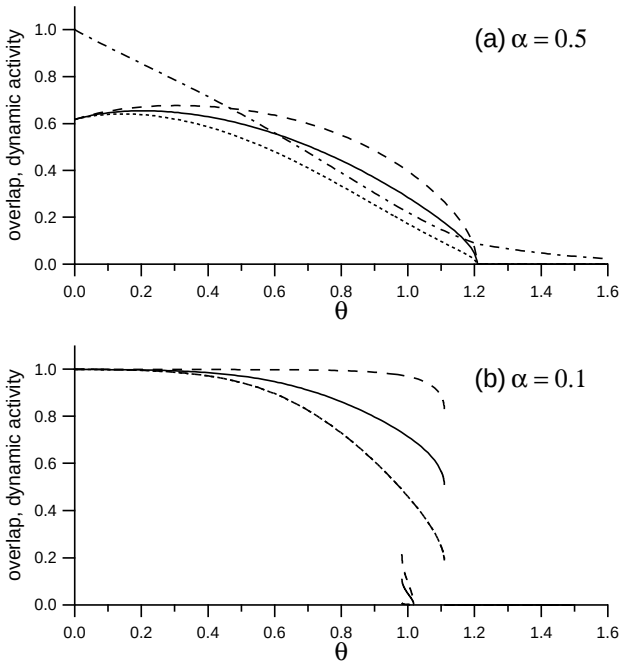

Fig. 2. M, $m_{\frac{1}{2}}$, m_1 and a_D as a function of θ for cuts across the phase diagram at the storage ratio values (a) $\alpha = 0.5$ and (b) $\alpha = 0.1$. Solid, dashed, dotted and dashed-and-dotted lines represent M, $m_{\frac{1}{2}}$, m_1 and a_D, respectively. The plot of a_D is indistinguishable from m_1 in Figure 2b, hence the dotted curve representing the latter is not visible.

For simplicity sake we assume that $a_\mu = a$ for all μ. Note that due to the bipartite character of the network the variables $m_{\frac{1}{2}}$ and m_1 are *explicit* functions of each other.

As for static properties, we are interested in plotting the phase diagram of variables $M = \frac{1}{2}\left(m_{\frac{1}{2}} + m_1\right)$ and a_D, where M is the global overlap with the network consisting of both subnetworks. There are three possible phases: a "retrieval" phase where $M > 0$, $a_D > 0$, a "chaotic" (or spin glass) phase where $M = 0$, $a_D > 0$ and a "zero" (or "paramagnetic") phase where $M = 0$, $a_D = 0$. Note that the case of $M = 0$, $a_D = 0$, with a_D defined above as the activity of the $S = 1$ subnetwork, should not be confused with the "zero" (or "paramagnetic") phase presented in the Yedidia's analysis [11] where a_D was defined as a global variable, since a part of our system is composed of $S = \frac{1}{2}$ neurons whose activities are always positive.

We will limit our analysis to the case $a = 1$. Let us consider the case of $m_{\frac{1}{2}} \geq 0$ and $m_1 \geq 0$. From equation (20) it follows that for $m_{\frac{1}{2}} > 0$ the variable m_1 takes positive values and that $m_1 = 0$ if $m_{\frac{1}{2}} = 0$. Thus, the search for the boundary between the regions with $M > 0$ and $M = 0$ is equivalent to that for the boundary between the regions with $m_{\frac{1}{2}} > 0$ and $m_{\frac{1}{2}} = 0$. The boundary between $a_D = 0$ and $a_D > 0$ is given by the condition that

$$\mathrm{erf}\left(\frac{m_{\frac{1}{2}} + \theta}{\sqrt{2\alpha}}\right) - \mathrm{erf}\left(\frac{m_{\frac{1}{2}} - \theta}{\sqrt{2\alpha}}\right) = 2 \qquad (23)$$

should be satisfied for $a_D = 0$. Equation (23) holds only if the values of θ attain infinity or are larger than $m_{\frac{1}{2}}$ with $\alpha = 0$. This means that, in contrast to the Yedidia's model [11], there is no effective "zero" phase ("paramagnetic") region in the phase diagram.

The phase diagram of $M(\alpha, \theta)$ or, equivalently, that of $m_{\frac{1}{2}}(\alpha, \theta)$, is given in Figure 1. In regions A and C, there is only one solution with nonzero M. In the region B, two solutions with nonzero M can coexist and which one is actually selected depends on the initial conditions. The region D corresponds to the "chaotic" phase; there is no overlap, but the final activity of the $S = 1$ subsystem remains finite. The solid line represents a second-order phase transition. The dashed and dotted lines represent the first-order phase transitions. In the case of $\theta = 0$, our model is equivalent to a network composed of two-state neurons. Indeed, the nonzero value of α at $\theta = 0$ is nearly equal to $2/\pi$, which is consistent with the result by Yedidia [11] at $\theta = 0$ and that by Derrida *et al.* [21].

To understand the phase diagram better, let us analyze its cuts at some values of α and θ. Figures 2a and 2b show the θ dependence of M, $m_{\frac{1}{2}}$, m_1 and a_D for $\alpha = 0.5$ and $\alpha = 0.1$, respectively. It can be found in Figure 2a that M attains its maximum value at $\theta \simeq 0.2$ and vanishes at $\theta \simeq 1.2$ in a continuous way characteristic of a second order phase transition. Figure 2b shows that there are two possible nonzero M solutions in the vicinity of $\theta = 1.0$. The solution with larger M decreases monotonically with the increase of θ and vanishes at $\theta \simeq 1.1$ in a way characteristic of a first order phase transition. Note that

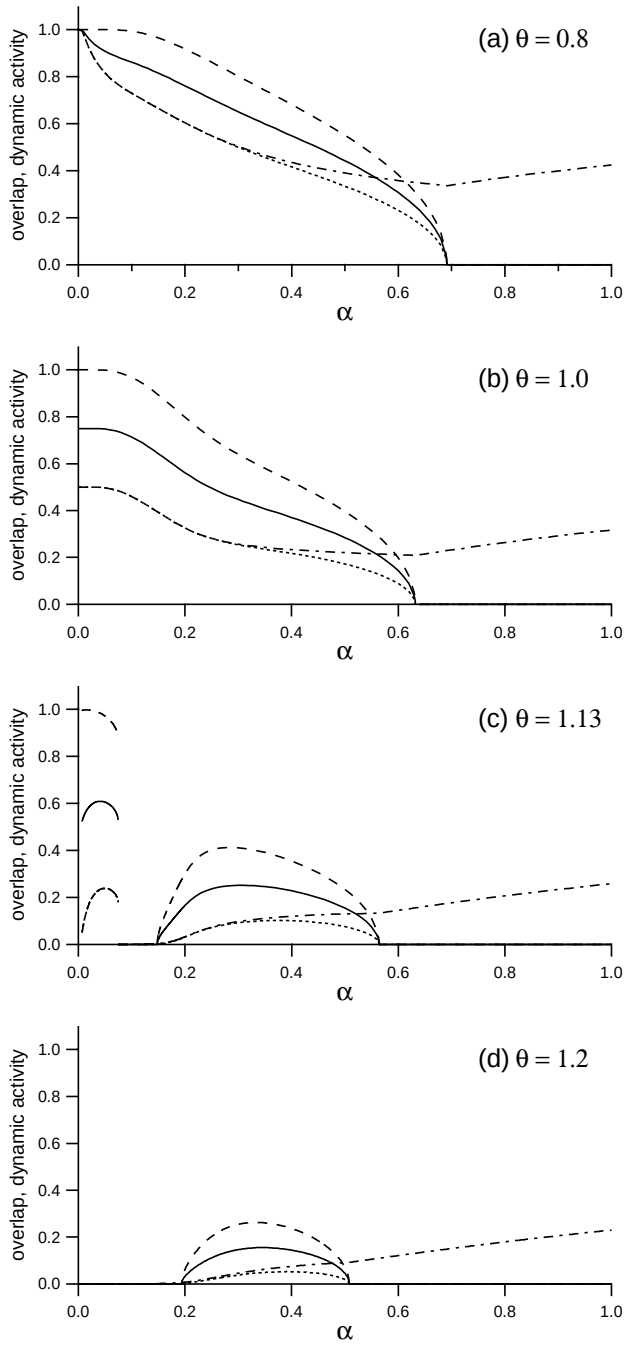

Fig. 3. M, $m_{\frac{1}{2}}$, m_1 and a_D as a function of storage ratio α for cuts across the phase diagram at (a) $\theta = 0.8$, (b) $\theta = 1.0$, (c) $\theta = 1.13$ and (d) $\theta = 1.2$. Solid, dashed, dotted and dashed-and-dotted lines represent M, $m_{\frac{1}{2}}$, m_1 and a_D, respectively. Note that for small α the dynamic activity a_D does not differ from m_1 in the scale of the figure.

the values of m_1 and a_D are so close that one can not distinguish them in the scale of Figure 2b.

In the phase diagram seen in Figure 1 two solutions can be found, *e.g.*, for $\theta = 0.8$ and $\theta = 1.0$. But the range of α in which two solutions for M coexist is very narrow. Therefore we concentrate on the analysis of the solutions with larger M only. Figures 3a, 3b, 3c and 3d show the overlaps M, $m_{\frac{1}{2}}$, m_1 and dynamic activity a_D as a function of α for $\theta = 0.8$, $\theta = 1.0$, $\theta = 1.13$ and $\theta = 1.2$, respectively. In the case of $\theta = 0.8$ (Fig. 3a) and $\theta = 1.0$ (Fig. 3b), we do not plot those solutions of $m_{\frac{1}{2}}$ and m_1 with smaller values, although they can exist. In Figure 3a, $m_{\frac{1}{2}}$, m_1 and M decrease monotonically with growing α; $m_{\frac{1}{2}}$, m_1 and a_D take the value 1.0 at $\alpha = 0$. Also in Figure 3b, $m_{\frac{1}{2}}$, m_1 and M decrease monotonically with α. At $\alpha = 0$, however, a_D is equal to 0.5, which means that half of the $S = 1$ neurons are off and therefore the value of m_1 is 0.5. In the case of $\theta = 1.13$, the overlap shows interesting features (Fig. 3c). There are two separate ranges of α in which nonzero solutions of overlap exist. In both ranges, the plots of the overlap as a function of α are convex curves. At $\theta = 1.2$, there is only one region in which nonzero solutions of the overlap exist (Fig. 3d). The maximum value of the overlap becomes small in that region. In Figures 3a, 3b, 3c and 3d, the values of m_1 and a_D differ but very slightly for small α, similarly as in Figure 2b. Hence, a separate plot of a_D is not visible in Figure 2b.

5 Dynamic properties

In the previous section, we found that two solutions with nonzero M can coexist in the region B and which state is reached by the network depends on the initial conditions $(m_{\frac{1}{2}}(0), m_1(0), a_D(0))$. In this section, we analyze dynamics of the network and discuss the basin of attraction for such two states. In the noiseless case, dynamic equations (16–18) are reduced to

$$m_{\frac{1}{2}}(t+1) = \mathrm{erf}\left(\frac{m_1(t)}{\sqrt{2\alpha a_D(t)}}\right), \tag{24}$$

$$\begin{aligned} m_1(t+1) &= \frac{1}{2}\left[\mathrm{erf}\left(\frac{m_{\frac{1}{2}}(t)-\theta}{\sqrt{2\alpha}}\right) + \mathrm{erf}\left(\frac{m_{\frac{1}{2}}(t)+\theta}{\sqrt{2\alpha}}\right)\right] \\ &\equiv f\{m_{\frac{1}{2}}(t)\} \end{aligned} \tag{25}$$

and

$$\begin{aligned} &a_D(t+1) \\ &= \frac{1}{2}\left[2 + \mathrm{erf}\left(\frac{m_{\frac{1}{2}}(t)-\theta}{\sqrt{2\alpha}}\right) - \mathrm{erf}\left(\frac{m_{\frac{1}{2}}(t)+\theta}{\sqrt{2\alpha}}\right)\right]. \end{aligned} \tag{26}$$

Note that we set $a_\mu = a$ for all μ for simplicity sake similarly as in the previous section. From equations (24–26) it follows that the dynamics of $m_{\frac{1}{2}}(t)$ obeys the equation of the form

$$m_{\frac{1}{2}}(t+2) = F\{m_{\frac{1}{2}}(t)\}. \tag{27}$$

With a set of parameters (θ, α) which belongs to the region B in the phase diagram (Fig. 1), the function $F(x)$

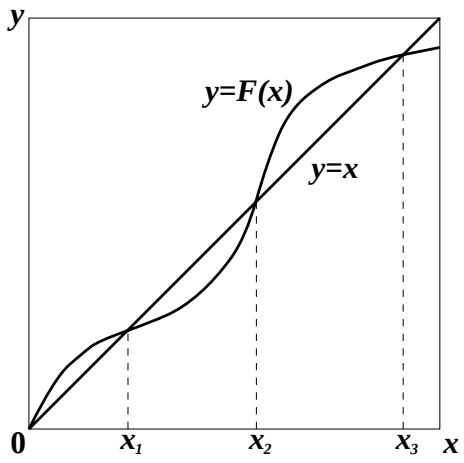

Fig. 4. The shape of the function $F(x)$, and the graphical representation of the solutions x_1, x_2, x_3 of $x = F(x)$ (see text).

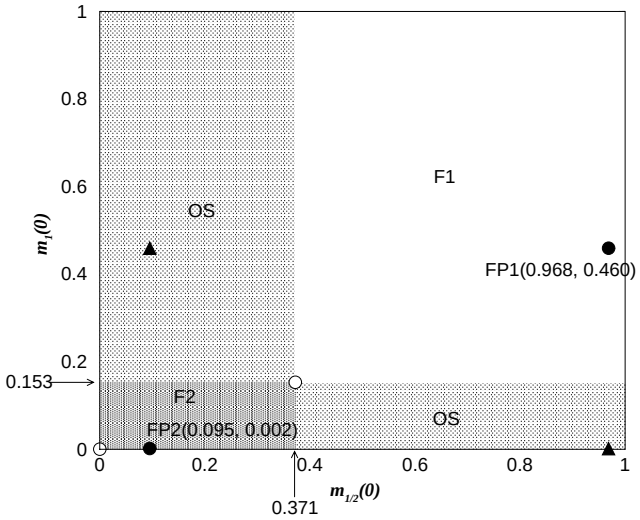

Fig. 5. The basins of attraction for the case $(\theta, \alpha) = (1.0, 0.1)$ and $a_D(0) = 1.0$. The region $F1$ is the basin of attraction for the fixed point $FP1(0.968, 0.460)$ and the same holds for the region $F2$ and the fixed point $FP2(0.095, 0.002)$. The two regions OS are basins of attraction for the oscillatory behavior of the system. The system oscillates between two states represented by two triangles in the figure. Two open circles are unstable fixed points.

has a shape drawn schematically in Figure 4. Let the solutions of $x = F(x)$ be $x = 0$, x_1, x_2, $x_3 (0 < x_1 < x_2 < x_3)$. According to the dynamic equation (27) and the Figure 4, the system at an even time step is expected to show several behaviors depending on the initial condition $m_{\frac{1}{2}}(0)$; (i) if $m_{\frac{1}{2}}(0) > x_2$, then $m_{\frac{1}{2}}(0)$, $m_{\frac{1}{2}}(2)$, $m_{\frac{1}{2}}(4), \ldots$ converge to x_3. (ii) if $m_{\frac{1}{2}}(0) = x_2$, then $m_{\frac{1}{2}}(0) = m_{\frac{1}{2}}(2) = m_{\frac{1}{2}}(4) = \ldots = x_2$. (iii) if $0 < m_{\frac{1}{2}}(0) < x_2$, then $m_{\frac{1}{2}}(0)$, $m_{\frac{1}{2}}(2)$, $m_{\frac{1}{2}}(4), \ldots$ converge to x_1. (iv) if $m_{\frac{1}{2}}(0) = 0$, then $m_{\frac{1}{2}}(0) = m_{\frac{1}{2}}(2) = m_{\frac{1}{2}}(4) = \ldots = 0$. On the other hand, behaviors of the system at an odd time step depend on $m_{\frac{1}{2}}(1)$, and $m_{\frac{1}{2}}(1)$ depends in turn on the initial condition $(m_1(0), a_D(0))$. For simplicity sake, from now on we restrict the initial dynamic activity $a_D(0)$ to be equal to unity. Now, let a solution of

$$x_i = \mathrm{erf}\left[\frac{x}{\sqrt{2\alpha}}\right], \quad i = 1, 2, 3 \tag{28}$$

be $\overline{x}_i$. We expect the following behaviors of the system at an odd time step: (i) if $m_{\frac{1}{2}}(1) > x_2$ (which corresponds to $m_1(0) > \overline{x}_2$), then $m_{\frac{1}{2}}(1)$, $m_{\frac{1}{2}}(3)$, $m_{\frac{1}{2}}(5), \ldots$ converge to x_3. (ii) if $m_1(0) = \overline{x}_2$, then $m_{\frac{1}{2}}(1) = m_{\frac{1}{2}}(3) = m_{\frac{1}{2}}(5) = \ldots = x_2$. (iii) if $0 < m_1(0) < \overline{x_2}$, then $m_{\frac{1}{2}}(1)$, $m_{\frac{1}{2}}(3)$, $m_{\frac{1}{2}}(5), \ldots$ converge to x_1. (iv) if $m_1(0) = 0$, then $m_{\frac{1}{2}}(1) = m_{\frac{1}{2}}(3) = m_{\frac{1}{2}}(5) = \ldots = 0$. Accordingly, if $m_{\frac{1}{2}}(0) > x_2$ and $m_1(0) > \overline{x}_2$, the system will converge to a fixed point $(x_3, f(x_3))$, and if $0 < m_{\frac{1}{2}}(0) < x_2$ and $0 < m_1(0) < \overline{x}_2$, the system will converge to another fixed point $(x_1, f(x_1))$. Furthermore, if $m_{\frac{1}{2}}(0) > x_2$ and $0 < m_1(0) < \overline{x}_2$, or if $0 < m_{\frac{1}{2}}(0) < x_2$ and $m_1(0) > \overline{x}_2$, the system will oscillate between two states, $(x_1, f(x_3))$ and $(x_3, f(x_1))$. The oscillatory behavior is well-known when the dynamics is parallel in a fully connected network [25].

The basins of attraction are shown in Figure 5 in the case of $(\theta, \alpha) = (1.0, 0.1)$ which belongs to the region B of the phase diagram. $(x_2, \overline{x}_2)$ is found to be $(0.371, 0.153)$ in the present case. Two fixed points are found to be $(0.968, 0.460)$ and $(0.095, 0.002)$; they are represented by filled circles in Figure 5. The system is attracted either to the fixed point $(0.968, 0.460)$ or $(0.095, 0.002)$, if it starts from an initial state $(m_{\frac{1}{2}}(0), m_1(0))$ either in the region $F1$ or in the region $F2$, respectively. On the other hand, the system which starts from an initial state in the region OS oscillates between two states $(0.968, 0.002)$ and $(0.095, 0.460)$, which are represented by filled triangles in Figure 5. Two points: $(0.371, 0.153)$ and $(0, 0)$ are unstable fixed points and they are drawn as open circles in Figure 5.

Solving the dynamic equations (24–26) numerically confirms the above discussion. Examples of time evolutions of the system in the case of $(\theta, \alpha) = (1.0, 0.1)$ are shown in Figure 6. As expected, when the system starts from an initial state lying within the region $F1$ or $F2$, it converges to fixed points $FP1$ or $FP2$, respectively (Figs. 6a and 6b). It is interesting that the system reaches the fixed points while oscillating. The system shows oscillatory behavior if it starts from an initial state lying within the region OS (Fig. 6c). Limit cycle attractors with length 2 are well-known in the fully connected networks of all neurons alike with little dynamics, but there the cycle consists of two embedded patterns. This contrasts with the situation encountered in our model where the cycle consists of two possible solutions for a single embedded pattern.

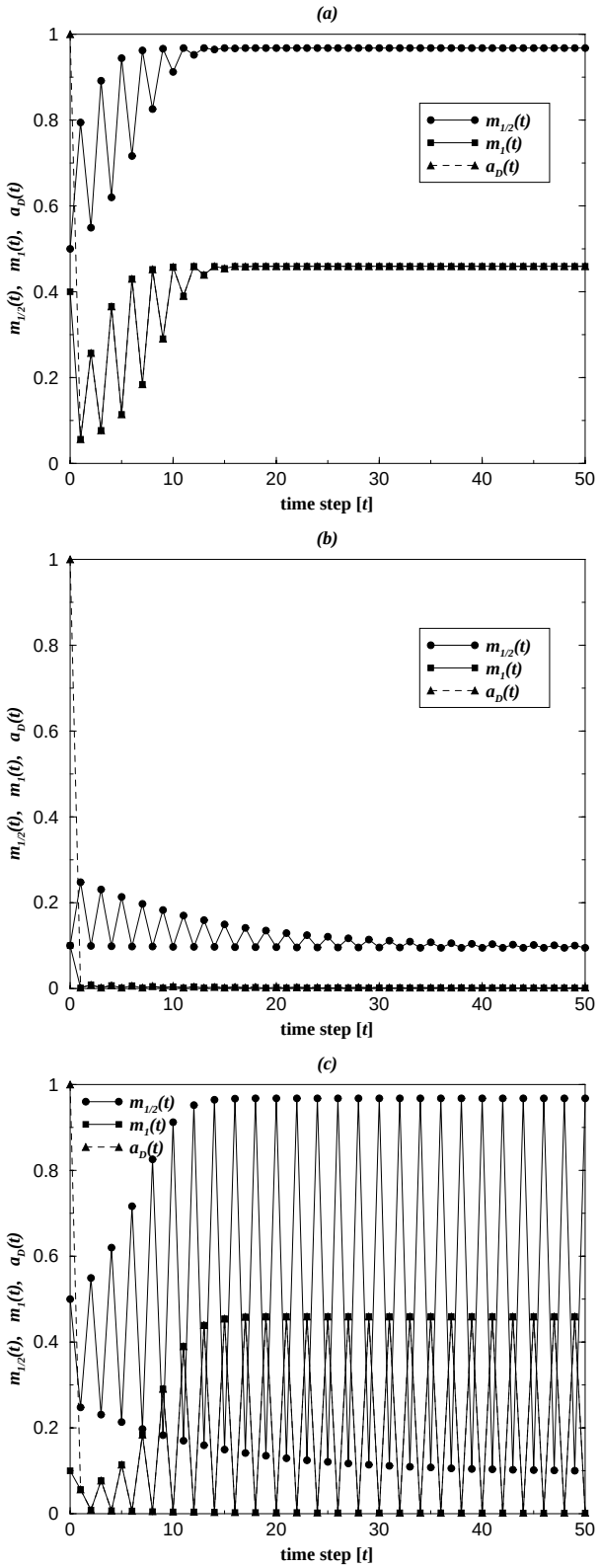

Fig. 6. Dynamics of the system starting from three different initial states $(m_{\frac{1}{2}}(0), m_1(0)) = (a)\ (0.5, 0.4)$, $(b)\ (0.1, 0.1)$, $(c)\ (0.5, 0.1)$. $a_D(0)$ is set equal to 0 in all cases. Time evolutions of $m_{\frac{1}{2}}(t)$, $m_1(t)$ and $a_D(t)$ are represented by a solid line with circles, a solid line with squares and a dashed line with triangles, respectively.

6 Summary

In this paper, we studied a neural network composed of both two-state and three-state neurons. Under the asymmetric dilution of synaptic connections and parallel dynamics, we have obtained, by standard methods, a set of equations describing the dynamics of the system. The equations had the form of recursion relations. A key point of our analysis was to calculate two kinds of overlap; one is the partial overlap of the subnetwork composed of two-state neurons with a given pattern and the other is that of the subnetwork composed of three-state neurons. The dynamic activity of the $S = 1$ subnetwork was also calculated.

In order to discuss static properties, we obtained the phase diagram, Figure 1, by solving dynamic equations at zero temperature in the equilibrium state. It was found that two kinds of fixed point solutions for overlap can coexist in a certain region, though the latter is rather narrow. Furthermore, in a certain range of θ, there are two separate ranges of α in which a nonzero overlap can exist (*cf.* Fig. 3c). To our knowledge, such a phase diagram with a gap between ranges of non-zero overlap has not been reported for neural networks with only two-neuron connections yet. On the other hand, this situation resembles some results presented by Arenzon *et al.* [26]. However, it should be remarked that the similarity mentioned above could be observed despite the fact that we have applied a different learning rule than that proposed in reference [26].

In order to consider dynamic properties of our system we have solved our dynamic equations numerically. As a result, we have found basins of attraction for two possible fixed points (Fig. 5). Also, the system is found to show oscillatory behavior when starting from an initial state belonging to a certain region in the parameter space (Fig. 6). In this case, the system oscillates between two possible solutions of the overlap for a single embedded pattern. This behavior contrasts with the oscillatory behavior observed in the dynamics of fully connected networks with a parallel updating rule and all neurons alike, since the latter type of oscillation consists of two embedded patterns.

The results presented here open some perspectives. For the case of a fully connected network, as contrasted to the asymmetrically diluted one discussed here, our model might be analyzed by some other methods, for example the replica theory [27] and the Self-Consistent Signal-to-Noise Analysis [28]. Still other extension would be a system having Q-state neurons ($Q > 3$) in place of three-state neurons applied in our present model. Within such an extended model, one could consider a system composed of mixed binary and analogue (with a continuous gain function) neurons, the latter treated in the limit of infinite Q. It would open a possibility of pattern recognitions for black-white and grey-toned patterns, forming for example the foreground and background, respectively.

References

1. J.J. Hopfield, Proc. Natl. Acad. Sci. USA **79**, 2554 (1982).

2. J.J. Hopfield, Proc. Natl. Acad. Sci. USA **81**, 3088 (1984).
3. C.M. Gray, P. Konig, A.K. Engel, W. Singer, Nature **338**, 334 (1989).
4. A.J. Noest, Europhys. Lett. **6**, 469 (1988); Phys. Rev. A **38**, 2196 (1988).
5. J. Cook, J. Phys. A **22**, 2057 (1989).
6. L.F. Abbot, J. Phys. A **23**, 3835 (1990).
7. T. Aoyagi, Phys. Rev. Lett. **74**, 4075 (1995).
8. I. Kanter, Phys. Rev. A **37**, 2739 (1988).
9. H. Vogt, A. Zippelius, J. Phys. A **25**, 2209 (1992).
10. D. Bollé, P. Dupont, J. Huyghebaert, Physica A **185**, 363 (1992).
11. J.S. Yedidia, J. Phys. A **22**, 2265 (1989).
12. J. Stark, P. Bressloff, J. Phys. A **23**, 1633 (1990).
13. H. Rieger, J. Phys. A **23**, L1273 (1990).
14. M. Bouten, A. Engel, Phys. Rev. E **47**, 1397 (1993).
15. Y. Nakamura, K. Torii, T. Munakata, Phys. Rev. E **51**, 1538 (1995).
16. R. Kühn, S. Bös, J.L. van Hemmen, Phys. Rev. A **43**, 2084 (1991).
17. Toru Aonishi, Koji Kurata, Masato Okada, `cond-mat/9808090`.
18. D. Bollé, P. Kozlowski, P. Kozłowski, J. Phys. A **31**, 6319 (1998).
19. T. Kaneyoshi, J. Phys. Soc. Jpn. **56**, 2886 (1987).
20. P. De Wilde, Phys. Rev. E **47**, 1392 (1993).
21. B. Derrida, E. Gardner, A. Zippelius, Europhys. Lett. **4**, 167 (1987).
22. R. Kree, A. Zippelius, in *Models of Neural Networks*, edited by E. Domany, J.L. van Hemmen, K. Schulten (Springer, Berlin, 1991), pp. 193.
23. D. Bollé, P. Dupont, J. van Mourik, Europhys. Lett. **15**, 893 (1991).
24. D. Bollé, P. Dupont, J. van Mourik, Physica A **185**, 357 (1992).
25. P. Peretto, *An Introduction to the Modeling of Neural Networks* (Cambridge University Press, Cambridge, 1992).
26. J.J. Arenzon, R.M.C. de Almeida, Phys. Rev. E **48**, 4060 (1993), and references therein.
27. D.J. Amit, H. Gutfreund, H. Sompolinsky, Ann. Phys. **173**, 30 (1987).
28. M. Shiino, T. Fukai, J. Phys. A **25**, L375 (1992).